Low-cost and Easy-to-Build Soft Robotic Skin for Safe and Contact-rich Human-Robot Collaboration

Kyungseo Park, Kazuki Shin, Sankalp Yamsani, Kevin Gim, and Joohyung Kim

***Abstract*—Although many soft robotic skins have been introduced, their use has been hindered due to practical limitations such as difficulties in manufacturing, poor accessibility, and cost inefficiency. To solve this, we present a low-cost, easy-to-build soft robotic skin utilizing air-pressure sensors and 3D-printed pads. In our approach, we utilized digital fabrication and ROS to facilitate the creation and use of the robotic skin. The skin pad was fabricated by printing thermoplastic urethane (TPU) and post-processed with an organic solvent to secure air-tightness. Each pad consists of a TPU shell and infill, so the internal air pressure changes in response to tactile stimuli such as force and vibration. The internal pressure is measured and processed by a microcontroller and transmitted to the PC via a serial bus. We conducted experiments to investigate the characteristics of the skin pads, and the results showed that the developed robotic skins are capable of perceiving interaction force and dynamic stimuli. Finally, we developed the dedicated soft robotic skins for our custom robot designed in-house, and demonstrated safe and intuitive physical human-robot interaction.**

***Index Terms*—Force and Tactile Sensing, Physical Human-Robot Interaction, Robot Safety, Additive manufacturing**

I. Introduction

INTEREST in collaborative robots has been emerging due to their versatility in improving daily human experiences. Since these robots could operate within an unstructured and cluttered environment, the robots may accidentally collide with nearby objects or people, causing a risk to human safety. This issue can be partially solved with several methods such as low-inertia structures [1], quasi-direct drive [2], and series-elastic actuator [3], [4]. If the robot has soft covers with a sense of touch, safety can be further improved.

Soft robotic skin would play an important role in physical human-robot interaction (pHRI) since it gives robots both mechanical compliance and tactile data simultaneously. The mechanical property of the soft material effectively mitigates the risk of physical contact, improving the intrinsic safety of the robots [5]. The tactile data can be used to enable active compliance [6] or social interaction [7], [8]. These key features are not only essential for safe and contact-rich human-robot collaboration but also available through soft robotic skins only. Therefore, it is desirable to utilize a whole-body soft robotic skin to enhance the robot's interaction capability.

Kyungseo Park was with the KIMLAB (Kinetic Intelligent Machine Lab), University of Illinois Urbana-Champaign, IL 61801, USA. He is now with the Department of Robotics and Mechatronics Engineering, Daegu Gyeongbuk Institute of Science and Technology (DGIST), Daegu 42988 South Korea (email: kspark@dgist.ac.kr)

All the other authors are with the KIMLAB (Kinetic Intelligent Machine LAB), University of Illinois Urbana-Champaign, IL 61801, USA. {kazukis2, yamsani2, kggim2, joohyung}@illinois.edu.

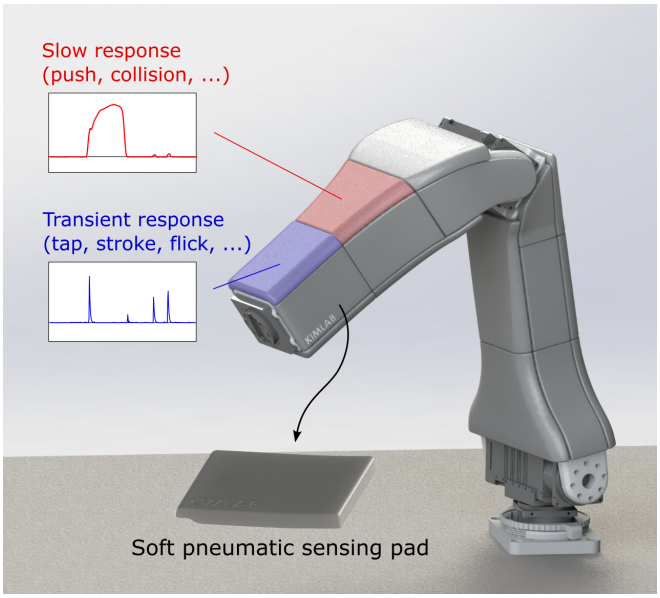

Fig. 1. Concept of the soft robotic skin. The robotic skin consists of soft pneumatic pads and sensing electronics. The developed robotic skin was able to sense slow (continuous) and transient (dynamic) tactile stimuli.

For this reason, there have been many studies to develop soft tactile sensors for robots. One of the practical approaches is to modularize tactile sensors using microcontrollers and serial communication [9], [10]. These small-sized modularized tactile sensors can be connected to each other via a serial bus, so they can be easily placed on a large and non-flat surface of the robot; this is a huge advantage considering that it is challenging to cover the entire surface of the robot with a large and monolithic soft tactile sensor. Nevertheless, it is not easy to perfectly fit the modules into the robot, making the system less complete than using a dedicated tactile sensor. In addition, fragile and exposed wiring could cause the sensor system to fail during physical interaction. It is also difficult to repair or replace the sensor if the modules and wires are molded in an elastomer.

Meanwhile, electrical impedance tomography (EIT) has also shown promising results in whole-body soft tactile sensing [11], [12]. This method measures the local impedance change on a large piezoresistive surface through distributed electrodes. Electric current is injected through various pairs of electrodes, and the resulting voltages are measured across the other electrodes. The tactile stimuli can then be reconstructed from the measurement data by using an inverse solver or deep neural network [13]. This approach has the advantage of scalability,

low production cost, and a simple and durable structure. However, the accessibility of this method is hindered by the need for a dedicated measurement device and the knowledge of EIT.

Other approaches using capacitance [14], optoelectric sensors [15], microphones [16], [17], or stereo cameras [18] have also been introduced with promising results, but they have not yet received widespread adoption as well; this might suggest that prioritizing practical factors, such as accessibility, cost efficiency, and production difficulty, is more important. If we could provide a durable, protective, and easily accessible whole-body robotic skin, it should facilitate various studies related to pHRI.

In this paper, we present a soft pneumatic robotic skin that consists of an air-filled soft pad and pressure sensor (see Fig. 1). This approach could be an attractive option due to the following advantages.

- Easy working principle
- Simple manufacturing process
- Use of off-the-shelf sensors
- Ease of achieving large-area coverage
- Durability and shock absorption capability

This approach has also been validated to be suitable for physical interaction due to its safe and durable structure [19], [20], so we aimed to make these sensors more accessible. The soft skin was 3D printed with an elastic material and additionally processed to ensure the air-tightness with a long lifespan. The shape of modular pads can be customized to thoroughly enclose the outer surface of the robot, and each pad can measure pressure change independently. The pressure data are measured and processed to distinguish a slow and transient response, and the data are transmitted to the PC via a serial bus. For demonstration, we developed the dedicated soft robotic skins seamlessly integrated into our custom robotic manipulator (PAPRAS) [21]. Then, we showed how the robotic skin could be used for pHRI, such as tactile servoing and commanding. Details and significance of the demonstration will be presented later.

This paper is organized as follows. Section II describes the overview of the developed robotic skin. The fabrication process is covered in section III. The characteristics of the robotic skin are presented in section IV with experiment results. Then, the usability of the developed soft robotic skin is validated through tangible demonstrations in Section V. Finally, the significance and limitations of our work will be discussed in Section VI.

II. Soft Pneumatic Robotic Skin

A. Design Requirements

In this work, we aimed to create practical robotic skins made with easily accessible machines (i.e., 3D printer, vacuum former). These machines are relatively inexpensive and have been owned and used by many facilities; this makes it easy for anyone to create their own custom robotic skin. Also, these machines could automate the manufacturing process and reduce manual labor; this can be a huge advantage considering that many soft robotic skins are handmade and require experience from each individual.

TABLE I
Design Requirements for Soft Whole-Body Robotic Skin

	Requirements
Manufacture	Digital modeling and fabrication, post-processing if needed
Durability	Resistant to collision, water, chemicals, pathogens, UV rays, ESD, etc.
Maintenance	Easy to repair, sanitize, and replace
Sensing modality	Continuous contact (sustained pressure) and transient contact (tap, flick, ...)
Resolution	Capable of rough contact localization

For reliability, we wanted to make our robotic skin resistant to various conditions such as collision, water, chemicals, pathogens, and Ultraviolet (UV). These conditions adversely affect the functions and long-term reliability of the soft robotic skin, limiting the use of tactile sensing systems in practical applications. To this end, we have used durable materials (TPU) while keeping the sensor structure as simple as possible. For instance, TPU is not only flexible but also resistant to chemicals (e.g., Clorox, water) and abrasion, allowing the robotic skin to keep its appearance, hygiene, and function under various conditions. We also tried to keep fragile components away from the external stimuli; only the soft pads are exposed to the external environment, and electronics such as wires and sensors are placed inside the robot. Details regarding the structure and fabrication of the robotic skin are described later.

For the sensing modality, we tried to make the robotic skin capable of sensing both continuous and transient responses. A continuous (sustained) response mostly represents an interaction force applied to the robot. A transient response corresponds to fast and instantaneous changes in pressure and usually encodes dynamic tactile stimuli or tactile events. Although such multi-modal sensing capability could be realized using heterogeneous transducers [11], [22], [23], we have utilized only one type of transducer (pressure sensor) and signal processing to simplify the structure and fabrication process.

For spatial resolution, we have decided not to pursue a precise contact localization performance. Form follows function; for example, the human finger has much higher spatial resolution than the back and thigh. These differences suggest that the whole-body physical interactions are more related to unsophisticated works rather than delicate tasks. For instance, Aimee et al. demonstrated that a soft robotic skin capable of rough contact localization allows the robot to grasp large objects using its body [24]. This result suggests that for whole-body robotic skin, mechanical compliance, and scalability are more critical than the capability for precise contact localization. The design requirements are summarized in Table I.

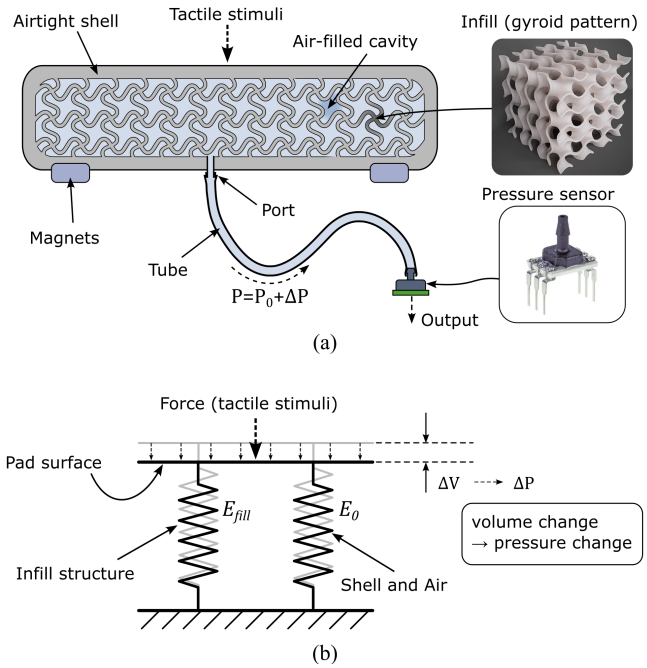

Fig. 2. (a) Structure and working principle of soft pneumatic sensor pad. The sensor pad is composed of an airtight shell, infill with the gyroid pattern, and an air-filled cavity. (b) Modeling of the soft pneumatic sensor pad.

B. Sensor Structure

The structure of the soft pneumatic pad is shown in Fig. 2. Each soft pneumatic pad consists of an airtight shell and mesh-like infill, which are made of TPU. The airtight shell prevents air leaks, so the internal pressure changes in response to deformation due to tactile stimuli. Each pad has a barbed port so it can be connected to the pressure sensor (ABPDANT005, Honeywell) through a urethane tube. The pressure sensors are located at the central sensing electronics, and the microcontroller (Teensy 4.0, PJRC) measures the pressure change due to contact.

The infill structure plays a crucial role in providing cushioning and tactile sensing capability to the soft pad. First, the infill supports the airtight shell and prevents excessive deformation of the sensing pad. Second, the infill structure imposes mechanical constraints on the soft shells. Without the infill structure, when the soft pad is poked, other parts of the pad would swell similar to an inflated balloon. This implies that the internal pressure might not change sufficiently, even under deformation. Third, the infill has a gyroid pattern, so the sensing pad could be strong yet light. Also, the gyroid pattern has no isolated space inside, thus the contacts can be measured at any location on the pad. This feature allows the robotic skin to achieve a large sensing area.

The characteristics of the soft pneumatic pad could also be customized by adjusting the printing parameters, such as infill density. For an infinitesimal area on the surface of the pad, the soft pneumatic pad can be roughly modeled as a set of vertical springs, as shown in Fig. 2. Each spring is corresponding to the infill structure and the air spring, respectively. The mechanical compliance of the soft pad is determined by the equivalent elastic modulus E_{eq}.

$$E_{eq} = E_{fill} + E_0 \tag{1}$$

where the constant E_0 is the elastic modulus due to the shell and air. The number E_{fill} is the modulus of the infill structure. These constants are determined by several factors, such as infill parameters, air volume, and initial internal pressure. For instance, the constant E_{fill} will be larger than E_0 if the infill is dense and stiff. Certainly, the properties may vary for each position of the soft pad due to potential non-uniformities in the printing process or location-specific variations in design. The effect of design parameters on mechanical compliance will be addressed in Section IV.

C. Working Principle

The developed soft pneumatic robotic skin perceives tactile stimuli by measuring the pressure changes inside the pad. The internal pressure P is related to volume and temperature as below.

$$PV = kT \tag{2}$$

where V, T are the volume and temperature of the air inside the pad, and k is constant. If we assume an adiabatic process, the internal pressure can be determined by the volume change as follows.

$$\frac{P_0 + \Delta P}{P_0} = \left(\frac{V_0 + \Delta V}{V_0}\right)^{-\gamma} \tag{3}$$

where P_0 and ΔP are the initial value and changes of the internal pressure, and V_0 and ΔV are the initial value and changes of the air volume. The constant γ is the heat capacity ratio of the air (typical value is 1.4). Then, the change in the internal pressure becomes

$$\frac{\Delta P}{P_0} = \left(1 + \frac{\Delta V}{V_0}\right)^{-\gamma} - 1 \tag{4}$$

This equation describes the relationship between the volume change and resulting pressure change during the adiabatic process.

On the other hand, the assumption of an adiabatic process holds only for a short time since heat exchange always takes place in the real environment. If the pad's volume changes slowly, the heat exchange will keep the internal air temperature the same as the shell and infill. Therefore, we also need to consider an isothermal process that leads to the following equation.

$$\frac{P_0 + \Delta P}{P_0} = \left(\frac{V_0 + \Delta V}{V_0}\right)^{-1} \tag{5}$$

Then, the change in the internal pressure becomes

$$\frac{\Delta P}{P_0} = \left(1 + \frac{\Delta V}{V_0}\right)^{-1} - 1 \tag{6}$$

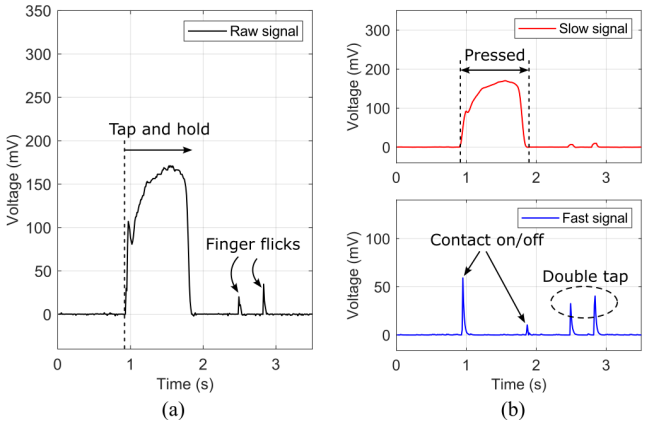

Fig. 3. (a) An example of raw signal measured from the pneumatic pad. The signal changes by the tactile stimuli (tap, hold, and finger flicks). (b) The raw signal is separated into slow (red) and fast (blue) components by micro-controller.

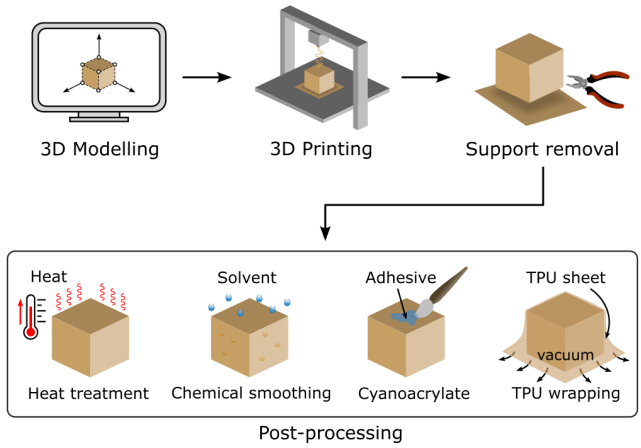

Fig. 4. (a) An example of raw signal measured from the pneumatic pad. The signal changes by the tactile stimuli (tap, hold, and finger flicks). (b) The raw signal is successfully separated into slow and fast components.

These equations imply that the soft pneumatic robotic skin may exhibit an overshoot-like behavior, which may cause an estimation error transiently. However, the significance of this effect will depend on the rate of heat exchange. For example, if heat exchange occurs rapidly, slow pressure change can be considered an isothermal process, while transient response can be amplified by an adiabatic assumption. This effect will be investigated in Section IV.

D. Signal Processing

The tactile stimuli consist of the continuous contact and the transient contact. We can measure such stimuli via various transducers, but we have applied signal processing to the air pressure since our primary goal was to keep the structure and fabrication of the robotic skin as simple as possible. This approach has been validated in applications such as distinguishing hard collisions from soft contacts [25]. The microcontroller measured the output voltages of 11 pressure sensors at a sampling rate of 1kHz for each channel. To extract a slow response, we processed the raw signals with a 1^{st} order low-pass filter with a cut-off frequency of 20Hz.

$$y_1[n+1] = \alpha_1 \cdot y_1[n] + (1-\alpha_1) \cdot x[n+1] \tag{7}$$

where the constant α_1 is the low-pass filter coefficient and the variables x and y_1 are the measured and the filtered signals, respectively. The resulting signals were less noisy, and mostly responded to relatively slow stimuli (i.e., push, poke), as shown in Fig. 3. The filtered signal was also not highly sensitive to transient and fast contacts such as a finger flick.

At the same time, we extract a transient response from the raw signal x using 1^{st} order high-pass filter as below.

$$y_2[n+1] = \alpha_2 \cdot y_2[n] + \alpha_2 \cdot (x[n+1] - x[n]) \tag{8}$$

where the constant α_2 is the high-pass filter coefficient for a cut-off frequency of 30 Hz. The filtered signal y_2 only responded to dynamic tactile stimuli. Subsequently, the signal y_2 was rectified and smoothed to quantify the amplitude of the transient response p.

$$p[n+1] = \alpha_3 \cdot p[n] + (1-\alpha_3) \cdot |y_2[n+1]| \tag{9}$$

where the constant α_3 is the smoothing coefficient. An example of raw signal and its filtering results are shown in Fig.3. The slow component represents the magnitude of the interaction force, while the fast component represents the dynamic stimuli such as a finger flick or double tap. Although the pneumatic tactile sensing method may have limited sensing bandwidth compared to piezoelectric materials or microphones, the result presents that the developed robotic skin is sufficient to sense dynamic tactile stimuli in a general pHRI scenario.

III. Manufacture Procedure

A. 3D printing

To simplify the manufacturing process, we have used a fused deposition modeling (FDM) 3D printer (E2, Raise3D) and a thermoplastic urethane (TPU) filament (NinjaFlex, Fenner Inc.). FDM is the most widely used 3D printing process due to its cost-efficiency and ease of use [26], but the output quality is not the best; the resulting prints are likely to have a rough surface or less detail due to relatively low printing resolution. It is also not easy to secure air-tightness since there can be a small gap between the layers. The stereolithography (SLA) 3D printer can also be an affordable option, but the prints often degrade over time as it is exposed to UV rays (i.e., sunlight). This reaction adversely affects the long-term reliability of prints, so the SLA-type printer was excluded.

The overall production process is expressed in Fig. 4. The STL model files were prepared using 3D CAD software (Solidworks, Dassault Systemes). The corresponding g-codes are generated by 3D slicing software (ideaMaker, Raise3D), which converts the STL files into parts consisting of shells

TABLE II
COMPARISON OF POST-PROCESSING METHODS

	Pros	Cons
Heat treatment	Easy, intuitive	Appropriate heating method required
Chemical smoothing	Excellent result	Safety risk, ventilation facility required
Cyanoacrylate	Easy, fast	Brittle, vulnerable to high temperature
TPU wrapping	Reliable result	Need for manual finishing

and infills. Then, the soft pads are printed with the following settings. The number of shells was set from 1 to 2.5, and the infill density was between 4% and 12%. For improved adhesion between TPU layers, the nozzle temperature was set to 255 °C. This value is higher than the recommended value; the filament might ooze, so retraction settings must also be configured. The feed rate was set to 20 mm/s to achieve better print quality. In addition, the flow rate of the filament for the shell was set to be slightly excessive (110 %) to prevent small gaps between each layer. This setting does not guarantee the air-tightness of the soft pad straight from the printer, but its quality is found to be sufficient when combined with a simple post-processing step.

B. Post-processing

FDM 3D printers melt plastic filaments and build them layer by layer. This approach can create imperfections that can cause air leaks. Most of large gaps can be prevented by optimizing the printer settings, but even small gaps can cause the sensor to malfunction. Therefore, it is required to remove the gaps through post-processing, such as heat treatment, chemical smoothing, super gluing, and TPU wrapping (see Table II). To achieve the desired quality, these methods can be repeated or used simultaneously. Heat treatment is the process in which heat is applied to the print to smooth the surface. The print is made of thermoplastic material (TPU), so the surface is melted due to heat and becomes smooth as they are cooled. Also, small holes can be naturally filled during the heat treatment. The heat can be applied using a heat gun, oven, or heating iron, which are easy to access. However, this method may cause some side effects; for example, the prints may burn if the applied temperature is too hot. Excessive heat for a long time also melts the internal infill structure and causes the print to collapse. In addition, bubbles may form on the print's surface from boiling moisture during heat treatment. This is because TPU print may retain moisture due to its hygroscopic property. Therefore, for successful heat treatment, it is necessary to find appropriate tools (e.g., iron, heating gun) and settings by trial and error.

Chemical smoothing is the process that uses the organic solvent to smooth the print's surface. The polymer starts to fill small gaps on the surface as they are dissolved in the solvents. Then, the defects are fixed as the solvent evaporates.

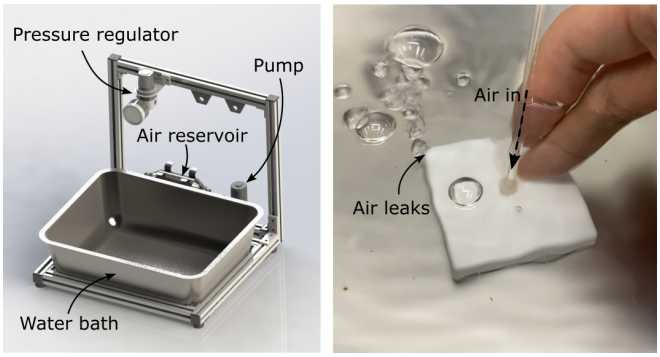

Fig. 5. (a) Inspection device for detecting small gaps that cause air leaks. It consists of a pump, air reservoir, pressure regulator, and water bath. (b) Air leaks through small defects and creates a bubble.

The solvents can be applied to the print through vaporing, dipping, and brushing. The usable solvent varies depending on the type of polymer, and the TPU can be used with solvents such as tetrahydrofuran (THF), dimethyl formamide (DMF), and dimethyl sulfoxide (DMSO). These organic solvents are often toxic or flammable and even form a peroxide with a risk of explosion, so they must be handled safely. However, this method will yield the best results if the proper facilities (i.e., safe container, ventilation) and protocols are in place.

Applying cyanoacrylate adhesives to the print's surface is also one of the easiest ways to fix small defects. When super glue (cyanoacrylate adhesive) is applied to the print's surface, the gap is filled, and air leakage stops. This method is easy to try because we can get the cyanoacrylate adhesive easily. However, since the adhesives are not resistant to high temperatures, the adhesive may fail due to heat. It may even release lethal gases when exposed to very high temperatures. Applying the superglue to the entire surface is also inconvenient, so this method may be best suited for fixing minor defects quickly.

The soft pad can also be wrapped with a TPU sheet using a vacuum former. This machine heats a thermoplastic sheet to make it pliable and pulls it around the mold using negative pressure (or vacuum). We used the vacuum former to conform the TPU sheet to the pneumatic pad. After that, we trimmed the edge and applied heat to fuse the pneumatic pad and the TPU film. This method guarantees air-tightness because the TPU sheet is inherently air-tight. Also, the use of vacuum former may help to automate the manufacturing process. Nevertheless, it was still required to manually finish the TPU sheet.

C. Inspection

Even after the post-processing, it might not be enough to guarantee the air-tightness of the pneumatic pad. Thus, we made an inspection device that could check for air leaks by putting a certain pressure of air into the pad (Fig. 5). Air was compressed using a miniaturized air pump (4404K25, McMaster-Carr), and stored in a small air reservoir (CRVZS-0.1, Festo). Compressed air was regulated to a pressure of 3 psi by an air regulator (6763K81, McMaster) and injected into the pneumatic pad. Then, the pads were placed in a water bath so that air bubbles were generated from the small gaps of the

pad. Once the defects were found, we could fix them by using soldering iron, instant adhesive, and organic solvent. For easy understanding, we demonstrated the process of inspecting a sample soft pad. The results can be found in Supplementary materials.

D. Production cost

The soft pneumatic pads are made of only TPU, so it has low production cost. For instance, a pneumatic pad measuring 90 mm by 60 mm by 10 mm consumes 34 g of TPU, which costs \$2.89. The magnets and barbed fitting also cost \$0.67, and \$0.57, respectively. Even adding the cost of post-processing, the total production cost of each pad is less than \$5. The pressure sensor and microcontroller cost around \$26 and \$23, and they are not required to be replaced or maintained as they are located inside the robot. In short, our soft robot skin requires an inexpensive initial cost, and its low replacement cost is advantageous for maintenance.

IV. Sensor Characteristics

A. Experiment Setups

We have conducted several experiments to investigate the characteristics of the soft pneumatic pads. The experiment setups are shown in Fig.6. The first setup has been used to conduct indentation experiments. The soft pneumatic pad measuring 50mm×50mm×10mm was placed on the top of the small cube and pressed by a rigid hemispherical tip with a radius of 7.5 mm. This tip was attached to the loadcell (FX29K, TE connectivity) located at the end of the rack, and the engaged pinion gear was actuated by a servo motor (XM430-W210, Robotis). During the experiment, the sensing electronics are used to log the indentation depth, force, and internal air pressure. This experiment was repeated several times for soft pneumatic pads with different infill densities.

The second setup has been used to conduct an impact experiment. The F/T sensor was attached to the fixture that is fixed to the metal frame. Four 500-gram weights (total 2kg) were mounted on a carrier printed with PLA. This carrier was connected to four strings(1.2m) and suspended from the overhead metal frame. A soft sensing pad was installed in front of the carrier, and it was detachable. Collision experiments were performed by releasing the mass carrier from a stationary state. After being released, the mass swung and collided with the F/T sensor at a specific speed, and the impact force was logged.

B. Force-pressure Curve

The relationships between the applied force and the resulting changes in air pressure are shown in Fig. 7. The maximum indentation depth was fixed to 4mm. The result shows that the modulus of the soft pads ranges from about 0.7 MPa and 2.9 MPa. The curves were monotonic and consistent, and the base pressure is not changed much since the ambient temperature has been constant. These results support the feasibility of the proposed tactile sensing method.

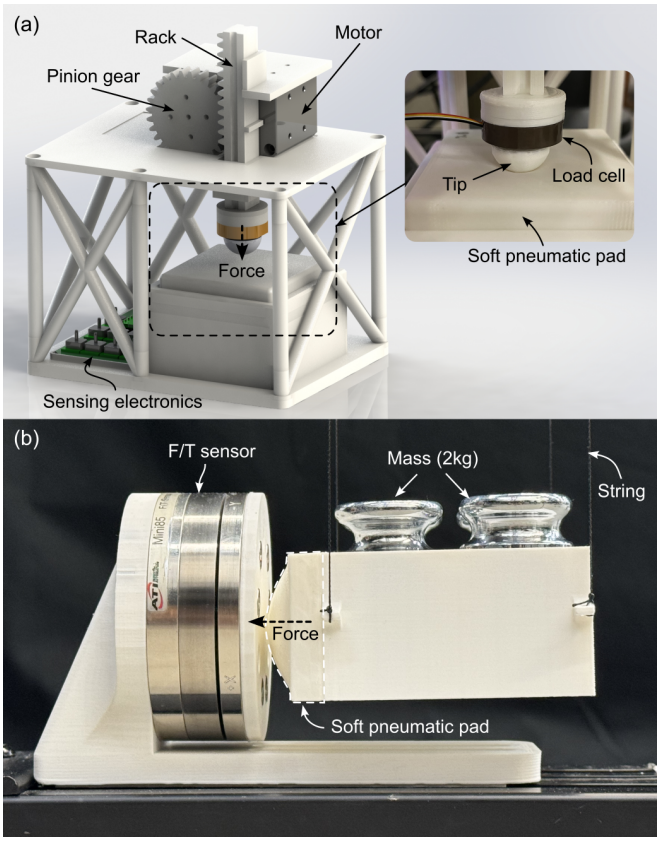

Fig. 6. (a) Indentation experiment setup is composed of servo motor, rack, pinion, loadcell, and hemi-spherical tip; (b) Impact experiment setup consists of F/T sensor, soft pad, mass, and string.

The hysteresis loops were also observed during the repeated indentation. This is due to the loss of energy in the mechanical deformation of the soft pad, and it can be quantified by the following equation.

$$Hysteresis(\%) = 100\left(\frac{W_{load} - W_{unload}}{W_{load}}\right) \quad (10)$$

where the value W_{load} and W_{unload} are the work during the loading and unloading. The result shows that the degree of hysteresis is about 10% to 15%. These numbers might not be ideal, but the usability of the sensor is not significantly compromised.

C. Mechanical compliance

The experiment result also presents the relationship between the infill density and the mechanical compliance of the soft pneumatic pad. As the infill density increases from 4% to 12%, the force value at the 4mm indentation depth increases from 10 N to 21 N while the maximum pressure changes also decrease from 4.9 kPa to 2.4 kPa. This means that the soft pad becomes harder as the infill density increases. To quantify the results, we assumed that the infill structure could be replaced with a set of vertical linear springs. Then, the soft pad's equivalent modulus can be calculated as follows.

$$E_{eq} = E_{fill}(\rho) + E_0 = \frac{F}{\Delta V} D_t \quad (11)$$

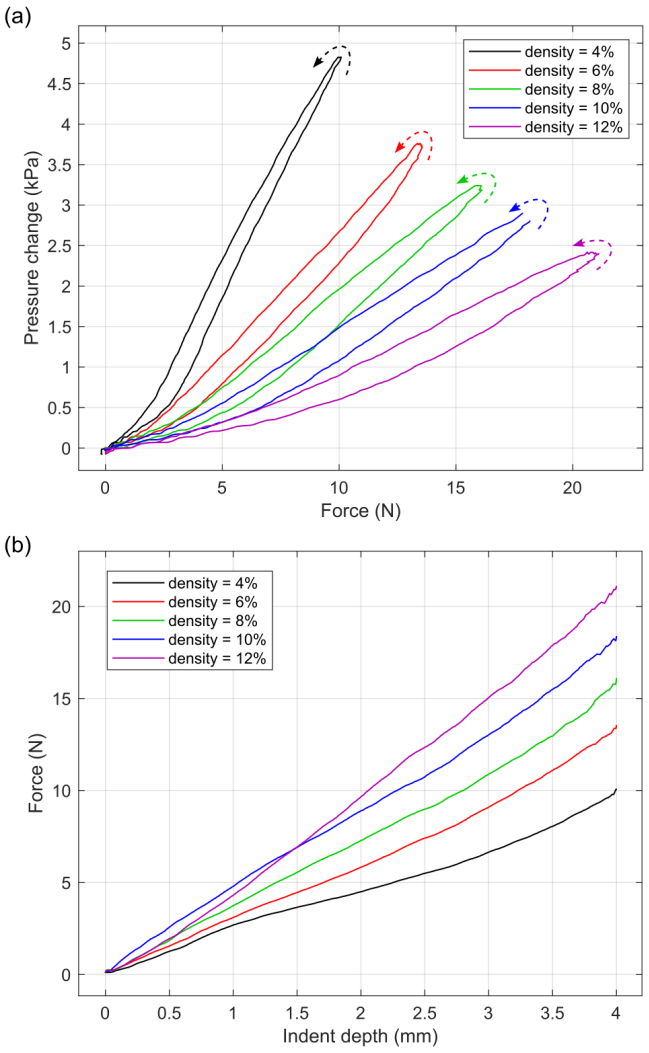

Fig. 7. (a) Relationship between the applied force and the resulting change in internal air pressure; (b) Relationship between the indentation depth and its reaction force.

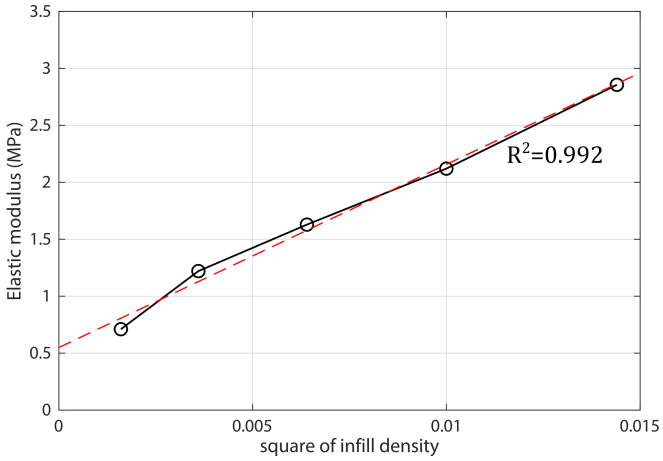

Fig. 8. Relationship between the infill density and the elastic modulus of the soft pneumatic pad. The black line and the red dashed line indicate the experimental values and the result of linear regression.

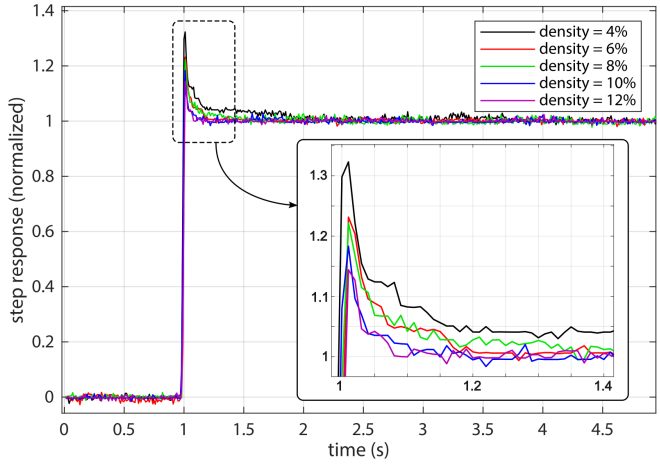

Fig. 9. Step response of the air pressure by indentation. The overshoot-like behavior was presented due to the changes in temperature during the adiabatic process, and it is settled due to the heat exchange.

where ρ and D_t are the infill density and the thickness of the soft pad, respectively. The modulus of the infill E_{fill} is found to be proportional to the square of the infill density ρ since the number ρ means the density of the infill structure along one axis. The volume change ΔV was calculated from the pressure value with an assumption of the isothermal process since the indentation was conducted at a rate of 0.01 Hz. The relationship between the infill density and the elastic modulus is shown in Fig. 8. The result reveals that the modulus increases linearly with respect to the square of the infill density. The constant term corresponds to the modulus by air and shell, and its value was about 0.55 MPa. These results imply that the mechanical property of the soft pneumatic pad can be adjusted if necessary.

D. Overshoot by Temperature Change

As the soft pad deforms, the internal temperature of the pad changes due to adiabatic assumption. However, this effect is valid only for a moment due to the heat exchange. It means that the pneumatic pad temporarily follows an adiabatic process, but in the long run, it follows an isothermal process. Therefore, the heat exchange rate will determine the characteristics of the soft pneumatic robotic skin.

To investigate this effect, we roughly estimated the thermal time constant of the soft pneumatic pad measuring 5cm x 5cm x 1cm. For the given condition, the heat capacity of the air becomes

$$\frac{dQ}{dT_{air}} = \rho V c_v \simeq 2.1\times10^{-2}\text{J/K} \tag{12}$$

where ρ, b, c_V are the density and volume of the air, and isometric specific heat of the air. If we assume an infill density of 8%, the heat transfer rate $\dot{Q}$ becomes

$$\dot{Q} = \frac{dQ}{dt} = hA\left(T_{pad} - T_{air}\right) \simeq 0.2\text{W/K} \tag{13}$$

where the number h is the heat transfer coefficient under free or weakly forced air convection. The number A is the contact

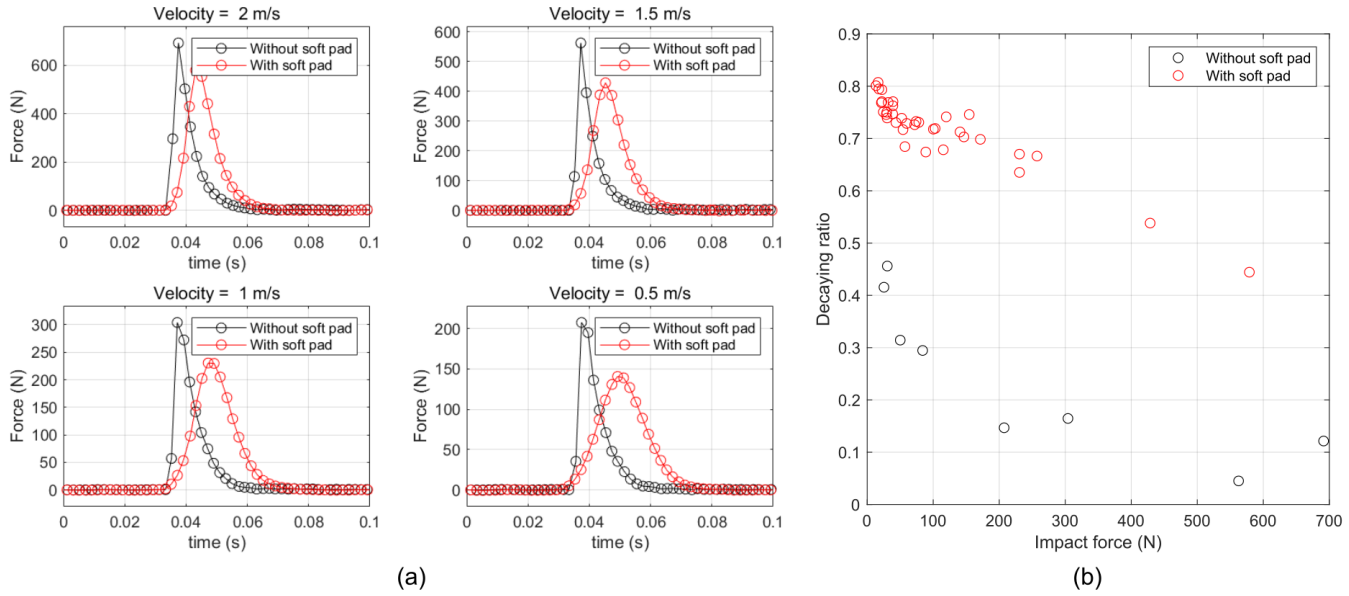

Fig. 10. (a) Force profile during the collision. The red and black graphs indicate the resulting force with and without the soft pad, respectively; (b) The ratio between the peak impact force and the impact force of the subsequent collision. A lower value indicates that a significant amount of the object's mechanical energy has dissipated.

area between the internal air and the soft pad including the shell and infill. The variables T_{pad} and T_{air} are the temperature of the soft pad and the inside air, respectively. Finally, we have a differential equation as follows.

$$\frac{dT_{air}}{dt} \simeq \frac{0.2\text{W/K}}{2.1\times10^{-2}\text{J/K}}\left(T_{pad} - T_{air}\right) \tag{14}$$

Since the heat capacity of the soft pad is significantly larger than the air, the T_{pad} was assumed to be constant. Then, the air temperature converges to T_{pad} as below.

$$T_{air}(t) = T_{pad} - \left(T_{pad} - T_{air}(0)\right)\exp\left(-\frac{t}{\tau}\right) \tag{15}$$

where the number τ is the thermal time coefficient that means the time to reach the temperature gradient equals 63% of the initial temperature gradient. The estimated thermal time constant is approximately 0.1s, and it can be varied by infill or convection conditions.

For validation, we obtained step responses of the pressure by indentation, and calculated the thermal time constant from the results, as shown in Fig. 9. The indentation depths were adjusted so that each specimen had the same settled value of pressure. The step responses are also normalized by settled values for comparison. The experiment result reveals that the time constant decreases from 0.24s to 0.027s as infill density increases. When the infill density was 8%, the resulting thermal time constant was 0.075s, which is somewhat similar to the estimated value (0.1s). After four times the time constant, about 98% of the overshoot is settled, meaning that the overshoot almost disappears within 0.3s for the pad with an 8% of infill density. This result suggests that the heat is exchanged rapidly inside the soft pad. Therefore, a relatively slow tactile stimulus can be considered to follow an isothermal process, meaning that a sustained force can be measured without any problem.

TABLE III
SUMMARY OF IMPACT EXPERIMENT

Soft skin	velocity (m/s)	0.5	1	1.5	2
without	peak force (N)	207	304	562	691
	time to peak (ms)	4.2	3.9	3.8	4.2
with	peak force (N)	140	230	429	579
	time to peak (ms)	9.9	11.9	13.9	17.7
change	peak force	-32%	-24%	-31%	-15%
	time to peak	+135%	+205%	+266%	+321%

E. Impact Experiment

The impact experiment results are shown in Fig. 10, and some key values are summarized in Table III. The Force profiles demonstrate that the soft pad effectively reduces the peak impact force by approximately 15% to 32%, and increases the time to reach peak force by about 2.35 to 4.21 times. These findings are consistent with the results of previous studies [19] and validate the efficacy of the soft pad in a collision. As the peak force is reduced, the risk of injuries, such as fractures, is mitigated. Additionally, a longer duration of collision provides enough time for the robot to react to the impact, thereby offering the potential to further reduce risks.

In addition, we observed how much the mass bounced after the collision and how the peak force was attenuated during the repeated collision (see Fig.10 b). The experiment results show that the mass almost comes to a stop after the first collision without a soft pad. Since the kinetic energy from the collision is converted into mechanical deformation, heat, and sound,

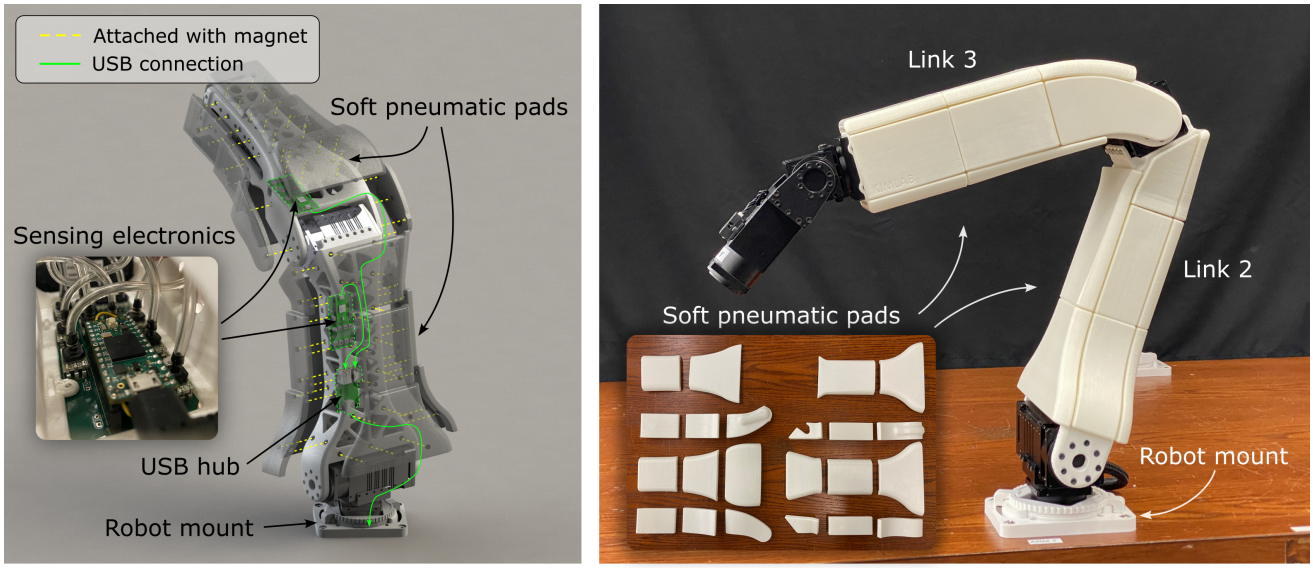

Fig. 11. (a) Rendered image of the robot arm integrated with dedicated soft pneumatic skins (exploded view). The green lines indicate the USB lines connecting the sensing electronics and the host. The dashed yellow lines show where the soft pad attaches to the robot arm via magnets. (b) Picture of the robot arm integrated with soft pneumatic robotic skin. This picture also shows soft pads arranged on a desk.

these results imply that significant physical damage would be inflicted on the object in a collision without the soft pad. In contrast, with the soft pad, the energy loss is significantly mitigated. Furthermore, we have observed that the soft pad exhibits mechanical hysteresis; these suggest that the soft pad not only reduces the risks of the collision but also absorbs some of the impact damage through its mechanical properties.

V. Demonstration of Whole-body Interaction

A. Hardware Integration

The soft pneumatic robotic skin has a simple structure and working principle, so it can be easily customized and produced by using 3D CAD design software and a 3D printer. To demonstrate this benefit, we developed a whole-body robotic skin for the plug-and-playable robotic arm system (PAPRAS). This robot arm was designed in-house and had the configuration of a typical 6-DoF articulated robot. The dedicated sensors are designed to achieve a sleek appearance and are attached to link 2 and 3. Each pad was fabricated by a 3D printer and post-processed by applying tetrahydrofuran (THF) to the surface (chemical smoothing). Then, a plastic barbed port was installed on each pad for the connection with the tube. Each pad was engraved with a circle for mounting magnets, and the magnets were secured with super glue.

The robot manipulator was also modified to accommodate the robotic skin. Similar to the soft pneumatic pad, magnets were installed on the surface of the robot arm. The links are designed to have an empty space where the central sensing electronics will be placed. The number of soft pneumatic pads was 11 as each PCB includes 11 pressure sensors. The pressure sensors are connected to the corresponding soft pneumatic pads via urethane tubes. The robot arm has holes and slots for the routing so that the tubes are not exposed to the outside. The microcontroller on each link was connected to a USB cable, and the cables were connected to the USB hub inside link 2. The upstream USB line of the hub was soldered to the connector located at the proximal end of the robot. So, the soft robotic skin was turned on automatically as the robot was inserted on the plug-and-playable mount.

The rendered image and the picture of the integrated system are shown in Fig. 11. The exploded view shows that the soft pneumatic pads are firmly attached to the robot manipulator via magnets. These magnets allow the soft pads to be freely attached and detached so that the sensor pads can be easily replaced in case of failure. The installation process of the soft robotic skin is demonstrated in Supplementary video 1. In addition, the sensor pad also improved the robustness and aesthetics of the system by covering the cables that had been exposed to the outside. This approach allows the robot to achieve whole-body tactile sensing capability without compromising the function or design of the original system.

B. Software Implementation

The soft robotic skin is integrated with the robot arm's software system for safe and intuitive pHRI. The robotic skin serves as a safety measure to prevent injury to the user or surrounding objects through mechanical compliance. The robotic skin also provides tactile information such as interaction force and tactile command for more natural and intuitive control of the robot arm. These features make it easier for users to control and interact with the robot.

The scheme of the overall software implementation is shown in Fig. 12. The main components for the software implementation are the microcontrollers, decision-making layer, motion planning layer, safety layer, controller, and hardware interface. The microcontrollers measured pressure values and conducted signal processing continuously. Then, the tactile data (interaction force and vibration) is sent to the host PC at a rate of 200

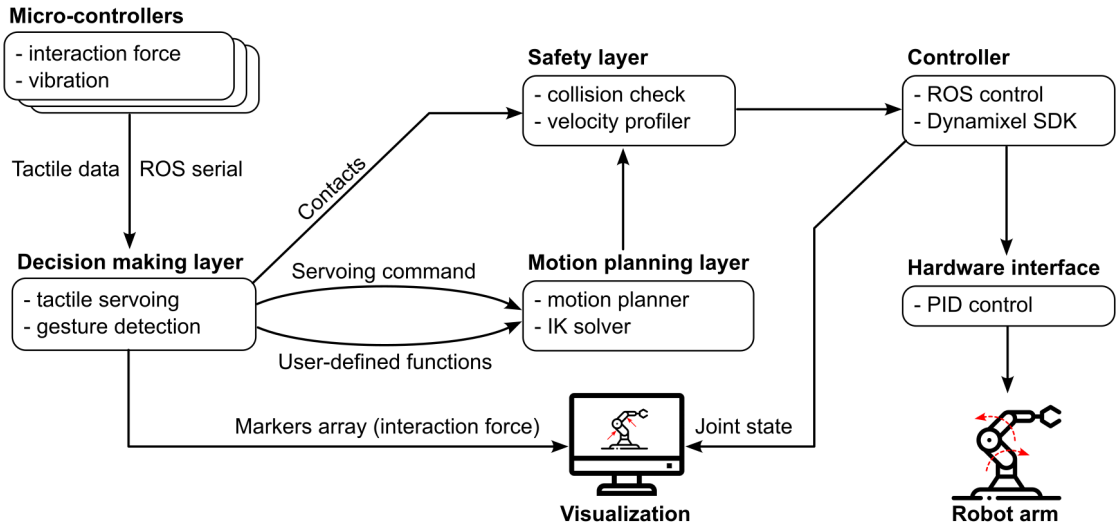

Fig. 12. Scheme of overall software implementation for the skin-integrated robot arm. The software system was implemented using ROS and MoveIt, and integrated with the micro-controllers and decision-making layer for tactile servoing and commanding.

Hz by using ROS serial library. The decision-making layer is responsible for determining which action is most appropriate given the interaction force from the robotic skin. For instance, the interaction force data (slow components) are used for tactile servoing and emergency stop, while the dynamic stimuli (i.e., double tap) are utilized to run user-defined functions through a gesture-recognition algorithm.

Next, the resulting commands are sent to the motion planning layer, which generates the target trajectory from the inputs through the motion planner and IK solver. The output trajectory is then sent to the safety layer, a part of the software stack responsible for detecting potential collisions and enforcing the joint limits of the robotic arm. The safety layer uses the 3D representation of the surrounding environment to detect potential collisions between the robot and other obstacles. If a collision is detected, the safety layer sends a signal to the robot's controller to stop its motion. This layer can also be implemented based on several approaches, such as feedback from the robotic skin, camera sensors, and odometry.

The controller layer provides commands to the robot to modify its behavior or trajectory. ROS control and Dynamixel SDK libraries are used to implement the hardware control loop for the robot system. The position controller is responsible for receiving and interpreting the commands from the planning and control system. It then sends the commands to the hardware interface, which is responsible for controlling the physical robot. The hardware interface uses the commands from the position controller to generate the necessary signals for the robot's actuators. This generates the desired motion for the robot, which is monitored by the position controller to ensure that the commanded motion is being followed correctly. If any errors occur, the position controller will inform the planning and control system, so the appropriate steps can be taken to correct the motion.

Concurrently, the sensor signals and control algorithms can be tested in a simulation environment before they are deployed in a real environment. The simulation was performed using Gazebo and visualized using Rviz. The decision-making layer published marker array messages that express the location and the level of the interaction force. Rviz also visualized the current location and pose of the robot by subscribing to the joint state sent from the controller. These features were used not only for simulation but also for visualizing the actual robot movement in real-time.

C. Physical Human-robot interaction

To present the usability of the developed robot skin, we demonstrated a safe and intuitive pHRI using interaction forces and dynamic stimuli. In this demo, the tactile data were used to implement tactile servoing and commanding. The tactile servo function was used for securing safety or direct teaching. Basically, the robot moves as usual when it has no physical contact with the external environment. If an interaction force is detected on the robot skin, the robot aborts the current task and enters tactile servo mode; the robot quickly stops and moves to reduce the interaction force caused by the collision.

The movement of the robot was determined based on the level and location of the interaction forces and the current pose of the robot [27]. For intuitive interaction, the joint motion was determined so that the pressed soft pad moved along the normal direction of its surface. The resulting joint motion becomes the least square solution because the relationship between the joint motion and target Cartesian motion is overdetermined. As the interaction force disappears, tactile servo mode is terminated so that the robot is ready to resume new tasks. This state transition makes it possible for the robot to move safely in emergency situations. Even if the tactile servoing is not performed quickly due to hardware limitations or communication latency, the soft pneumatic pad effectively handles residual risks through its mechanical compliance.

Next, we could give commands to the robot through physical contact. For example, the developed robot skin could recognize dynamic stimuli, such as a single or double tap. The robot counted the number of taps and performed a

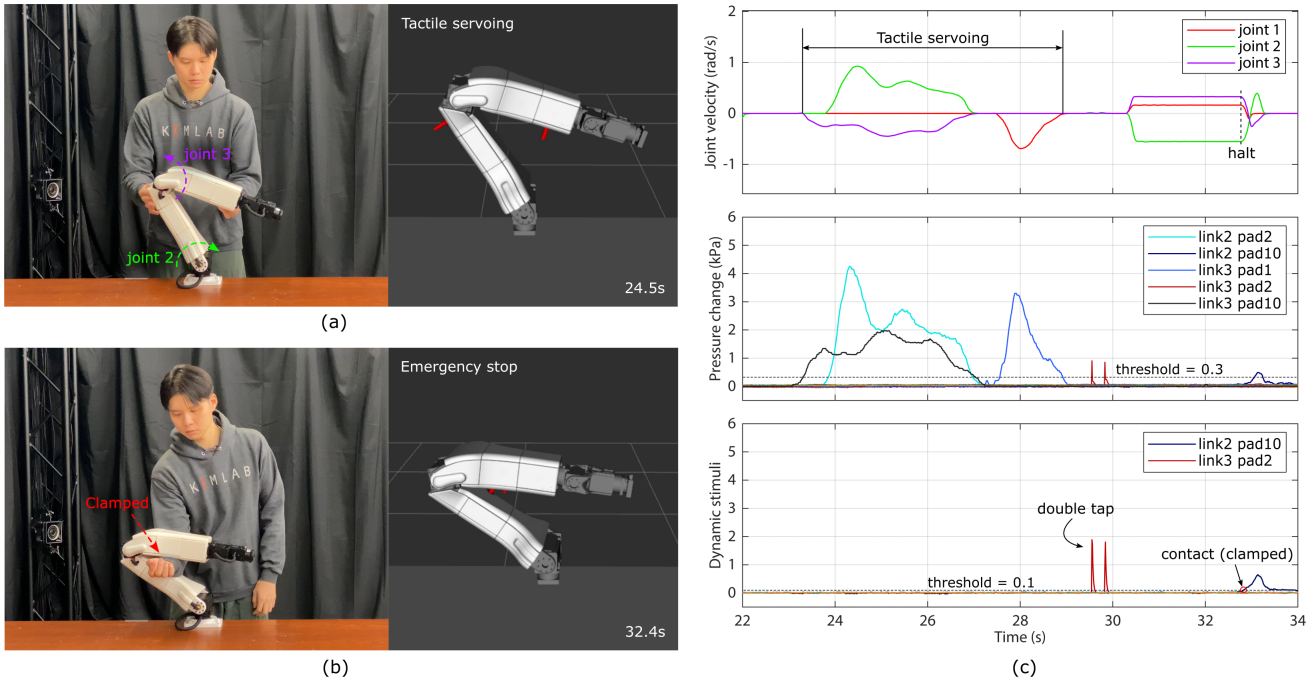

Fig. 13. Demonstration of safe and intuitive physical human-robot interaction through soft pneumatic robotic skin. (a) Whole-body tactile servoing using interaction force. The red arrows indicate the presence of interaction force applied to the robot. (b) Emergency stop of the robot by interaction force due to body clamping. (c) Joint velocity and tactile data were recorded during the demonstration.

predefined command accordingly. The single tap was used to stop the robot for safety (emergency stop) as it can happen unintentionally. Double and triple taps usually happen with intention, so we assigned them to functions that move the robot toward the home pose or folded pose. Even if these functions are accidentally initiated, the safety of the robot can be secured by the tactile servo mode.

Figure 13 presents an example scenario in which these features would work in the real environment. The full demo can be found in Supplementary Video 2. From 23 to 29 seconds, the robot was moved by pushing the robot directly with the hand. The servo commands were sent when an internal pressure change was larger than 0.3 kPa. After tactile servoing, the user tapped the robot twice at 29 seconds to move it into a folded position. The folded pose was predefined and could be changed if necessary. The motion from an arbitrary pose to the folded pose was planned using MoveIt [28]. These results show that the robot skin can be used as an input device for effective communication.

While the robot moves to the folded pose, the user intentionally causes a dangerous situation by putting his arm between the links. As the arm was clamped between the links, the robotic skin recognized the resulting interaction force and immediately halted the motion at around 32.4s. Then, the robot enters tactile servoing mode. Notably, there was a little delay (about 0.1s) in this reaction but the mechanical compliance of the soft pneumatic pad effectively prevented the accident. This result suggests the importance of achieving both passive and active compliance in pHRI.

VI. Discussion

The soft robotic skin can serve as an essential component for enabling human-robot collaboration, but it has not been widely utilized due to a lack of accessible options. To overcome this limitation, we proposed low-cost and easy-to-build soft robotic skin based on digital fabrication and the pneumatic tactile sensing method. This approach makes the production process simple and cost-competitive. Also, we expect that anyone can easily incorporate the proposed robot skin into their own projects due to its simple working principle and ROS-based software implementation.

As a proof-of-concept, we developed the dedicated robotic skin for our customized robot arm and integrated them on both the hardware and software side seamlessly. The integrated system was fully functional without compromising the functionality of existing robotic arms. The sensing electronics were ROS-enabled so that they could be easily stacked on the robot's software system. We demonstrated how tactile data can be utilized for physical interaction with a robot (see Supplementary video 2). The demonstration shows that the whole-body tactile data can be leveraged to realize safe and contact-rich pHRI.

We have also conducted an impact experiment to investigate the efficacy of the soft pad in ensuring safety during collision tests. The experiment results revealed that the soft pad provides protective functions in terms of peak force, duration of collision, and restitution (energy dissipation) during impacts. Several works suggest that safe and contact-rich interaction can be realized by modifying actuators and control algorithms; however, our results are highly accessible and do not require significant modifications to existing robots. Furthermore,

whole-body robotic skins provide clear benefits in dealing with multi-point contact and joint entrapment (clamping), as we demonstrated in this work.

Although our soft pneumatic robotic skin has shown promising results, it somewhat lacks in aspects such as spatial resolution and measurable modalities compared to other works. Therefore, it would be desirable for our robotic skin to be further improved for better usability. For example, the spatial resolution could be enhanced by either increasing the number of soft pads or creating multiple cavities within a single pad. In addition, proximity sensing capabilities could be easily incorporated with the use of conductive TPU filament. Nevertheless, to ensure that our current outcomes remain aligned with our research motivation, we must maintain the accessibility of the robot skin.

Next, the gesture recognition algorithm can also be enhanced. We only implemented a function that counts the number of taps, which is done independently for each sensing pad. The robot could be more versatile if the robotic skin is capable of understanding the spatio-temporal pattern of the tactile stimuli obtained from the entire surface of the robot. It would be beneficial to introduce a neural network for fully exploiting tactile data. Then, such improvement will be of great help to non-verbal communication.

ACKNOWLEDGMENT

Toyota Research Institute provided funds to support this work.

REFERENCES

[1] Y.-J. Kim, "Anthropomorphic low-inertia high-stiffness manipulator for high-speed safe interaction," *IEEE Transactions on robotics*, vol. 33, no. 6, pp. 1358–1374, 2017.

[2] D. V. Gealy, S. McKinley, B. Yi, P. Wu, P. R. Downey, G. Balke, A. Zhao, M. Guo, R. Thomasson, A. Sinclair *et al.*, "Quasi-direct drive for low-cost compliant robotic manipulation," in *2019 International Conference on Robotics and Automation (ICRA)*. IEEE, 2019, pp. 437–443.

[3] K. Haninger, A. Asignacion, and S. Oh, "Safe high impedance control of a series-elastic actuator with a disturbance observer," in *2020 IEEE International Conference on Robotics and Automation (ICRA)*. IEEE, 2020, pp. 921–927.

[4] H. Zhong, X. Li, L. Gao, and C. Li, "Toward safe human–robot interaction: A fast-response admittance control method for series elastic actuator," *IEEE Transactions on Automation Science and Engineering*, vol. 19, no. 2, pp. 919–932, 2021.

[5] J.-J. Park, S. Haddadin, J.-B. Song, and A. Albu-Schäffer, "Designing optimally safe robot surface properties for minimizing the stress characteristics of human-robot collisions," in *2011 IEEE International Conference on Robotics and Automation*. IEEE, 2011, pp. 5413–5420.

[6] E. Dean-Leon, J. R. Guadarrama-Olvera, F. Bergner, and G. Cheng, "Whole-body active compliance control for humanoid robots with robot skin," in *2019 International Conference on Robotics and Automation (ICRA)*. IEEE, 2019, pp. 5404–5410.

[7] R. B. Burns, H. Lee, H. Seifi, R. Faulkner, and K. J. Kuchenbecker, "Endowing a nao robot with practical social-touch perception," *Frontiers in Robotics and AI*, p. 86, 2022.

[8] S. Yohanan and K. E. MacLean, "The role of affective touch in human-robot interaction: Human intent and expectations in touching the haptic creature," *International Journal of Social Robotics*, vol. 4, no. 2, pp. 163–180, 2012.

[9] G. Cheng, E. Dean-Leon, F. Bergner, J. Rogelio Guadarrama Olvera, Q. Leboutet, and P. Mittendorfer, "A comprehensive realization of robot skin: Sensors, sensing, control, and applications," *Proceedings of the IEEE*, vol. 107, no. 10, pp. 2034–2051, 2019.

[10] A. Schmitz, P. Maiolino, M. Maggiali, L. Natale, G. Cannata, and G. Metta, "Methods and technologies for the implementation of large-scale robot tactile sensors," *IEEE Transactions on Robotics*, vol. 27, no. 3, pp. 389–400, 2011.

[11] K. Park, H. Yuk, M. Yang, J. Cho, H. Lee, and J. Kim, "A biomimetic elastomeric robot skin using electrical impedance and acoustic tomography for tactile sensing," *Science Robotics*, vol. 7, no. 67, p. eabm7187, 2022.

[12] K. Park and J. Kim, "Neural-gas network-based optimal design method for ert-based whole-body robotic skin," *IEEE Transactions on Robotics*, vol. 38, no. 6, pp. 3463–3478, 2022.

[13] H. Park, K. Park, S. Mo, and J. Kim, "Deep neural network based electrical impedance tomographic sensing methodology for large-area robotic tactile sensing," *IEEE Transactions on Robotics*, vol. 37, no. 5, pp. 1570–1583, 2021.

[14] P. Maiolino, F. Mastrogiovanni, G. Cannata *et al.*, "Skinning a robot: Design methodologies for large-scale robot skin," *IEEE Robotics & Automation Magazine*, vol. 23, no. 4, pp. 150–159, 2016.

[15] A. Cirillo, F. Ficuciello, C. Natale, S. Pirozzi, and L. Villani, "A conformable force/tactile skin for physical human–robot interaction," *IEEE Robotics and Automation Letters*, vol. 1, no. 1, pp. 41–48, 2015.

[16] M. J. Yang, K. Park, and J. Kim, "A large area robotic skin with sparsely embedded microphones for human-robot tactile communication," in *2021 IEEE International Conference on Robotics and Automation (ICRA)*. IEEE, 2021, pp. 3248–3254.

[17] D. Hughes and N. Correll, "Texture recognition and localization in amorphous robotic skin," *Bioinspiration & biomimetics*, vol. 10, no. 5, p. 055002, 2015.

[18] L. Van Duong *et al.*, "Large-scale vision-based tactile sensing for robot links: design, modeling, and evaluation," *IEEE Transactions on Robotics*, vol. 37, no. 2, pp. 390–403, 2020.

[19] J. Kim, A. Alspach, and K. Yamane, "3d printed soft skin for safe human-robot interaction," in *2015 IEEE/RSJ International Conference on Intelligent Robots and Systems (IROS)*. IEEE, 2015, pp. 2419–2425.

[20] A. Alspach, J. Kim, and K. Yamane, "Design of a soft upper body robot for physical human-robot interaction," in *2015 IEEE-RAS 15th International Conference on Humanoid Robots (Humanoids)*. IEEE, 2015, pp. 290–296.

[21] J. Kim, D. C. Mathur, K. Shin, and S. Taylor, "Papras: Plug-and-play robotic arm system," 2023. [Online]. Available: https://arxiv.org/abs/2302.09655

[22] P. Mittendorfer and G. Cheng, "Humanoid multimodal tactile-sensing modules," *IEEE Transactions on robotics*, vol. 27, no. 3, pp. 401–410, 2011.

[23] N. Wettels, J. A. Fishel, and G. E. Loeb, "Multimodal tactile sensor," in *The Human Hand as an Inspiration for Robot Hand Development*. Springer, 2014, pp. 405–429.

[24] A. Goncalves, N. Kuppuswamy, A. Beaulieu, A. Uttamchandani, K. M. Tsui, and A. Alspach, "Punyo-1: Soft tactile-sensing upper-body robot for large object manipulation and physical human interaction," in *2022 IEEE 5th International Conference on Soft Robotics (RoboSoft)*. IEEE, 2022, pp. 844–851.

[25] E. Mariotti, E. Magrini, and A. De Luca, "Admittance control for human-robot interaction using an industrial robot equipped with a f/t sensor," in *2019 International Conference on Robotics and Automation (ICRA)*. IEEE, 2019, pp. 6130–6136.

[26] M. H. Hasan, J. A. Sagor, and I. Agarwala, "A systematic trend analysis of 3d printing techniques used in specific soft robotic elements," *Materials Today: Proceedings*, vol. 50, pp. 1088–1099, 2022.

[27] T. Laliberté and C. Gosselin, "Low-impedance displacement sensors for intuitive physical human–robot interaction: Motion guidance, design, and prototyping," *IEEE Transactions on Robotics*, 2021.

[28] D. Coleman, I. Sucan, S. Chitta, and N. Correll, "Reducing the barrier to entry of complex robotic software: a moveit! case study," *arXiv preprint arXiv:1404.3785*, 2014.

Kyungseo Park (Member, IEEE) is currently an Assistant Professor of the Department of Robotic and Mechatronics Engineering, Daegu Gyeongbuk Institute of Science and Technology (DGIST). His research interests include physical human–robot interaction, tactile sensors, and interactive robots. He received the B.S., M.S., and Ph.D. degrees in mechanical engineering from Korea Advanced Institute of Science and Technology (KAIST), Daejeon, South Korea, in 2016, 2018, and 2022, respectively. He was a Postdoctoral Researcher in the Coordinated Science Laboratory, University of Illinois Urbana-Champaign from 2022 to 2023.

Kazuki Shin is currently working as a Computer Vision and Machine Learning Engineer at NVIDIA Corporation. He received a B.S. and M.S. degrees in Computer Engineering from the University of Illinois Urbana Champaign (UIUC), Champaign, IL, USA, in 2021 and 2023. His research interests include the perception and decision-making of autonomous systems.

Sankalp Yamsani (Student Member, IEEE) received his B.S degree in Computer Engineering from the University of Illinois Urbana-Champaign, Champaign, IL, USA in 2021. He is currently working on his M.S in Electrical and Computer Engineering at the University of Illinois Urbana-Champaign, Champaign, IL, USA. His research interests include robotics, robot perception, and human-robot interaction.

Kevin Genehyub Gim (Member, IEEE) is currently a Staff Mechanical Engineer at Boston Dynamics. He received a B.S. in Mechanical Engineering at Yonsei University, South Korea, an M.S. in Mechanical Engineering at the University of California, Los Angeles, USA, and a Ph.D. in Mechanical Engineering at the University of Illinois Urbana-Champaign, USA. His research interest is in developing mechanisms for legged robots, biped robots, humanoids, and human-robot interaction.

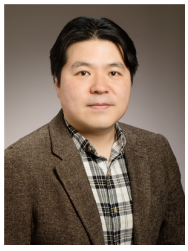

Joohyung Kim (Member, IEEE) is currently an Associate Professor of Electrical and Computer Engineering at the University of Illinois Urbana-Champaign. His research focuses on data/task-driven robot system design and interaction, including limbed robot design optimization, robot motion retargeting and learning, and seamless human-robot interaction. He received BSE and Ph.D. degrees in Electrical Engineering and Computer Science (EECS) from Seoul National University, Korea, in 2001 and 2012. He was a Research Scientist in Disney Research from 2013 to 2019. Prior to joining Disney, he was a postdoctoral fellow in the Robotics Institute at Carnegie Mellon University for the DARPA Robotics Challenge in 2013. From 2009 to 2012, he was a Research Staff Member in Samsung Advanced Institute of Technology, Korea, developing biped walking controllers for humanoid robots.